

Electronic Supporting information for the paper "On-Surface Synthesis of Polyethylenedioxythiophene"

Iolanda Di Bernardo,[a,c] Peter Hines,[b] Maryam Abyazisani,[c] Nunzio Motta,[b,c] Jennifer MacLeod [b,c †] and Josh Lipton-Duffin[b,c]

Detailed Experimental Methodology

Sample Preparation: Single crystal metal samples were cleaned by repeated cycles of Ar^+ bombardment at 1 keV for 10 minutes, followed by 10 minutes of annealing at 400°C, until no residual contaminants of carbon or oxygen could be detected by SRPES. DCEDOT was purchased from Tokyo Chemical Industry (>98.0%) and was used without further refinement. The molecule was deposited onto the cleaned surfaces through a high-precision leak valve. Surface coverages in Langmuir were calculated by the apparent pressure rise during molecular deposition, though the gauge used to record the pressure was not modified from its default calibration (for nitrogen). A residual gas analyser (SRS RGA100) was used to monitor the mass species of the background gas during dosing, to ensure that the observed pressure rise corresponded to DCEDOT-related mass fragments, rather than spurious readings due to air or contamination.

Photoemission and x-ray absorption spectroscopy: SRPES was performed at the Soft X-Ray (SXR) spectroscopy beamline of the Australian Synchrotron. All experiments were performed using linearly polarized light with a PHOIBOS 150 electron energy analyzer (SPECS GmbH) in normal emission geometry, with the incident radiation falling on the sample surface at an angle of 55° to the sample normal. The excitation energy for all core levels was $h\nu$=400 eV, except for the oxygen 1s line which was measured using $h\nu$=850 eV. Binding energies are referenced to the Fermi level, which was measured at each of the experimental steps. Carbon K-edge NEXAFS experiments were performed over a range of incidence angles with respect to the sample normal, from grazing incidence (p-polarisation, with the electric field vector inclined 20° from the sample normal) to normal incidence (s-polarisation, with the electric field vector parallel to the surface plane), using swept photon energies in the range from $h\nu$=270 eV to $h\nu$=320 eV. NEXAFS data were treated using the QANT routines[1] in Igor Pro (Wavemetrics). Spectra were double normalized against the incoming photon flux by measuring the current from a gold mesh in the path of the beam, and against spectra collected over the same energy range from a pristine substrate.

Scanning probe microscopy: STM experiments were performed at room temperature in UHV by using an Omicron VT-AFM/XA system with electrochemically etched tungsten tips. Bias voltages are reported from the tip to the sample. Images were processed using the free WSxM software.[2]

Calculations: DFT calculations were performed using the projector-augmented wave (PAW) pseudopotentials in Quantum ESPRESSO[3] under the generalized gradient approximation (GGA) with Perdue-Burke-Ernzerhof (PBE) parameterization for the exchange-correlation functional.[4] The exchange correlation was modified by adding an ab initio nonlocal van der Waals correlation contribution (vdW-DF), which is known to improve the description of the long-range dispersive forces of the standard GGA.[5] The Ag(111) surface was modeled using a 7-layer slab, holding the bottom three layers fixed and allowing the top four layers to relax. These top four layers were then used to model the absorption of PEDOT at high-symmetry sites. A vacuum gap of 10 Å was used to prevent communication of the molecules in the top layer with the Ag atoms of the bottom layer. The unit cell used for the geometry optimization was a (1 -2 | 6 2) cell ($2\sqrt{7}\times\sqrt{7}$ R40), as implied by STM images. The Brillouin zone was paved with a 3×2×1 k-point grid during the optimization, and this was increased to 20×10×1 to produce the simulated STM images. The latter were performed in the Tersoff-Hamann formalism,[6] with an additional Gaussian blurring to simulate the finite radius of the STM tip.

DCEDOT on Cu(111) – O 1s, Cl 2p and S 2p core levels

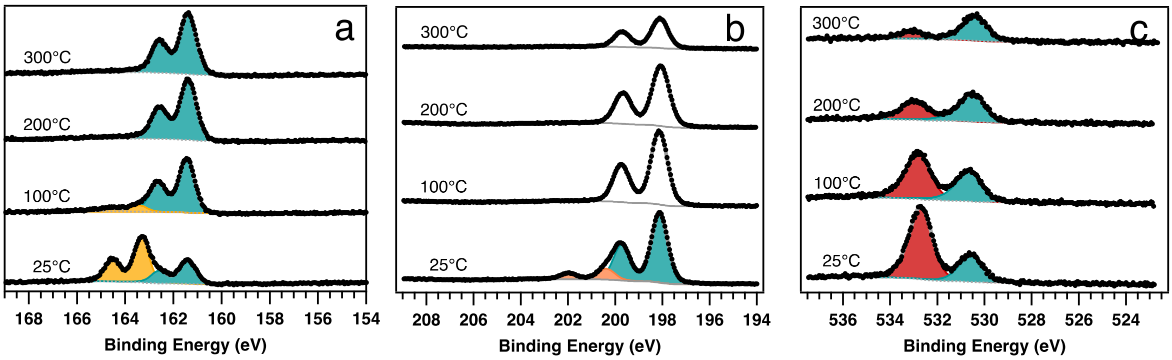

Figure 1: Core level spectra for DCEDOT on Cu(111), stacked as a function of annealing temperature for a) S 2p, b) Cl 2p, and c) O 1s.

Inspection of the O1s core level spectra in Figure 1c indicates that substantial decomposition of the molecule occurs immediately upon adsorption of DCEDOT onto the Cu surface; the presence of lower-BE states of oxygen (530.5 eV) indicates that these heteroatoms are abstracted from the molecule to form a metal oxide.

The Cl 2p spectra in Fig. 1b show that a small fraction of molecules remain halogenated at RT (pink doublet, Cl $2p_{3/2}$= 200.35 eV). We also find a lower-BE doublet (blue, Cl $2p_{3/2}$=198.1 eV) which we associate with metal-chloride arising from Cl atoms detached from the molecular precursor. We attribute the retained halogen to a reorientation of the molecule following the rupture of the thiophene ring, which would orient one of the α-carbons away from the surface, preserving the C-Cl bond. This rupture of the EDOT thiophene ring on Cu(111) is clearly recognized in the S2p spectra of Figure 1a: starting from RT, the high BE doublet ($S2p_{3/2}$ at 163.3 eV), originating from S in the intact molecule, is accompanied by another doublet at lower BE ($S2p_{3/2}$ at 161.4 eV) that we assign to S-Cu bonds. After the first annealing step the first of these two components is essentially eliminated, confirming the abstraction of sulfur from all EDOT moities.

DCEDOT on Au(111) – O 1s, Cl 2p and S 2p core levels

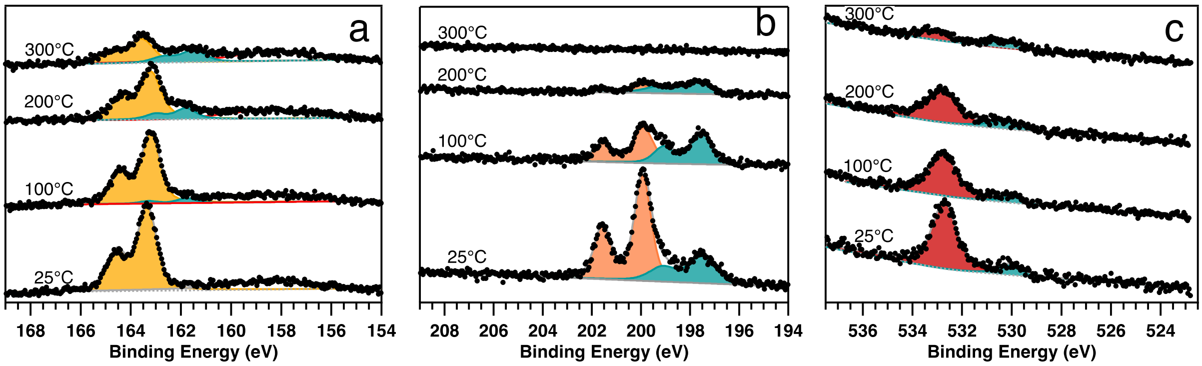

Figure 2: Core level spectra for DCEDOT on Au(111), stacked as a function of annealing temperature for a) S 2p, b) Cl 2p, and c) O 1s.

The S 2p spectra (Figure 2a) show that at room temperature the thiophene ring is intact, with only the molecule-related peaks present in the spectrum. Following annealing, the metal-associated low BE doublet emerges and increases in intensity, and the overall weight of the spectral region is reduced, suggesting fragmentation and desorption.

The spectral shape of the Cl 2p doublet on Au(111) (Figure 2b) indicates a partial dehalogenation of the monomer when adsorbed on the substrate at room temperature. As the surface is annealed the metal-associated (green) chlorine peak does not grow significantly, indicating that chlorine atoms detached from the monomer through the heating process are likely desorbed into the vacuum.

The oxygen core level on Au(111) is of rather weak intensity, and time-dependent studies (see below) seem to indicate that the synchrotron beam causes a fragmentation of the DCEDOT around the oxygen atoms. This would seem to explain the low signal intensity and is consistent with previous reports on non-halogenated precursors.

DCEDOT on Ag(111) – O 1s, Cl 2p and S 2p core levels

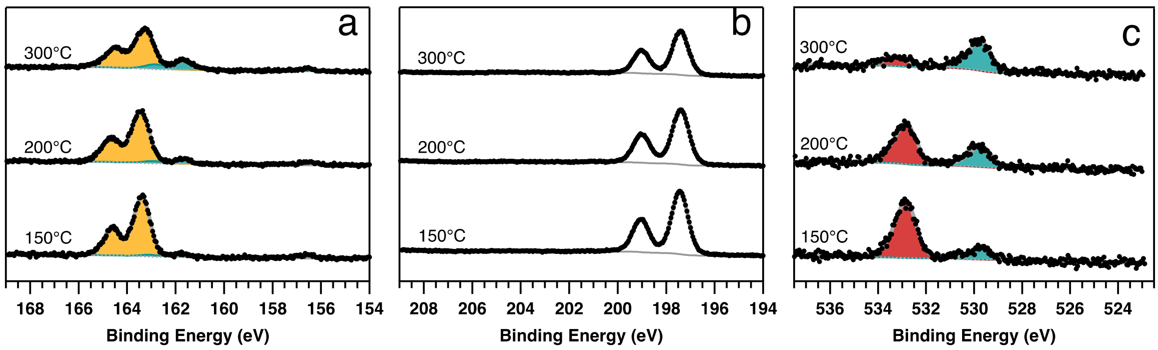

Figure 3: Core level spectra for DCEDOT on Ag(111), stacked as a function of annealing temperature for a) S 2p, b) Cl 2p, and c) O 1s.

After deposition onto the heated surface, the Cl 2p spectrum (Figure 3b) contains only the metal-coordinated state, indicating complete dehalogenation upon adsorption; the dehalogenative chemisorption is activated by the high substrate temperature, and mitigates the difficulty in sticking the molecule to Ag(111) at room temperature. Both the S 2p (Figure 3a) and O 1s (Figure 3c) show predominantly EDOT-related character upon deposition. As the sample is annealed the sulfur retains a thiophene-like character, with no significant growth of the metal sulfide state, but the oxygen signal progressively trades spectral weight for the metal-oxide state. This is consistent with the loss of the ethylene-C and β-C peaks in the carbon 1s shown in the main text.

DCEDOT on Au(111) – effect of beam damage

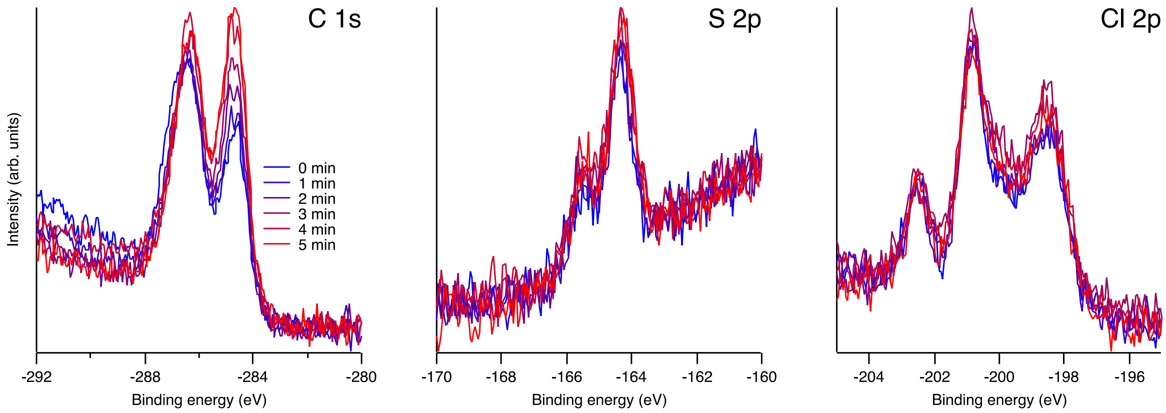

Figure 4: Beam damage effects of DCEDOT on Au(111)

A beam damage study was carried out on the DCEDOT monolayer deposited on Au(111). Figure 4 shows the evolution of the C 1s core level under continuous exposure to the synchrotron beam, immediately after deposition. An attenuation of the high-binding energy feature is observed, and the spectral weight is transferred to the low-binding energy side. The change in C 1s is accompanied by a lack of evolution in the S 2p and Cl 2p core levels, and we thus interpret the change as a fragmenting of the monomer at the oxygen-containing tail of the molecule.

NEXAFS spectra from all substrates

Spectra collected using linearly polarized light with a 55° tilt of the electric field vector with respect to the sample normal (the so-called magic angle), on Cu(111), Au(111) and Ag(111) are shown in The NEXAFS spectra presented in this plot correspond to the surfaces just after the 100°C annealing step (for Cu and Au), and immediately after deposition at 150°C for Ag. It is evident that the signature of intact EDOT is obtained only for the Ag(111) surface, with sharp resonances observed at photon energies of 285.8 eV, 286.9 eV and 289.4 eV, respectively labeled α, β, and γ in Figure 5. These resonances cannot be readily identified on either of the other two substrates at any incidence angle, and lends credence to the hypothesis that the molecule does not adsorb intact on Cu or Au.

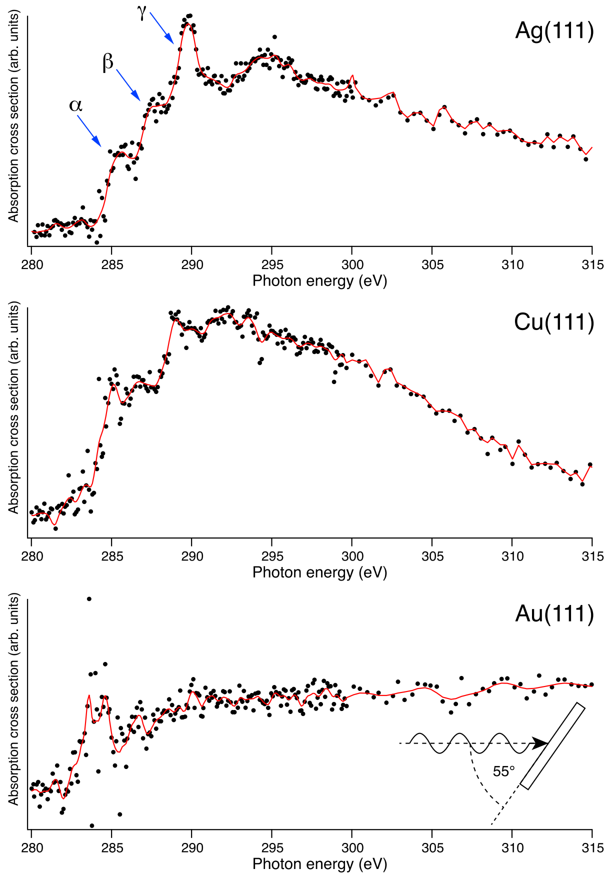

Figure 5: NEXAFS at the carbon K-edge for DCEDOT adsorbed on Ag, Cu, and Au surfaces.

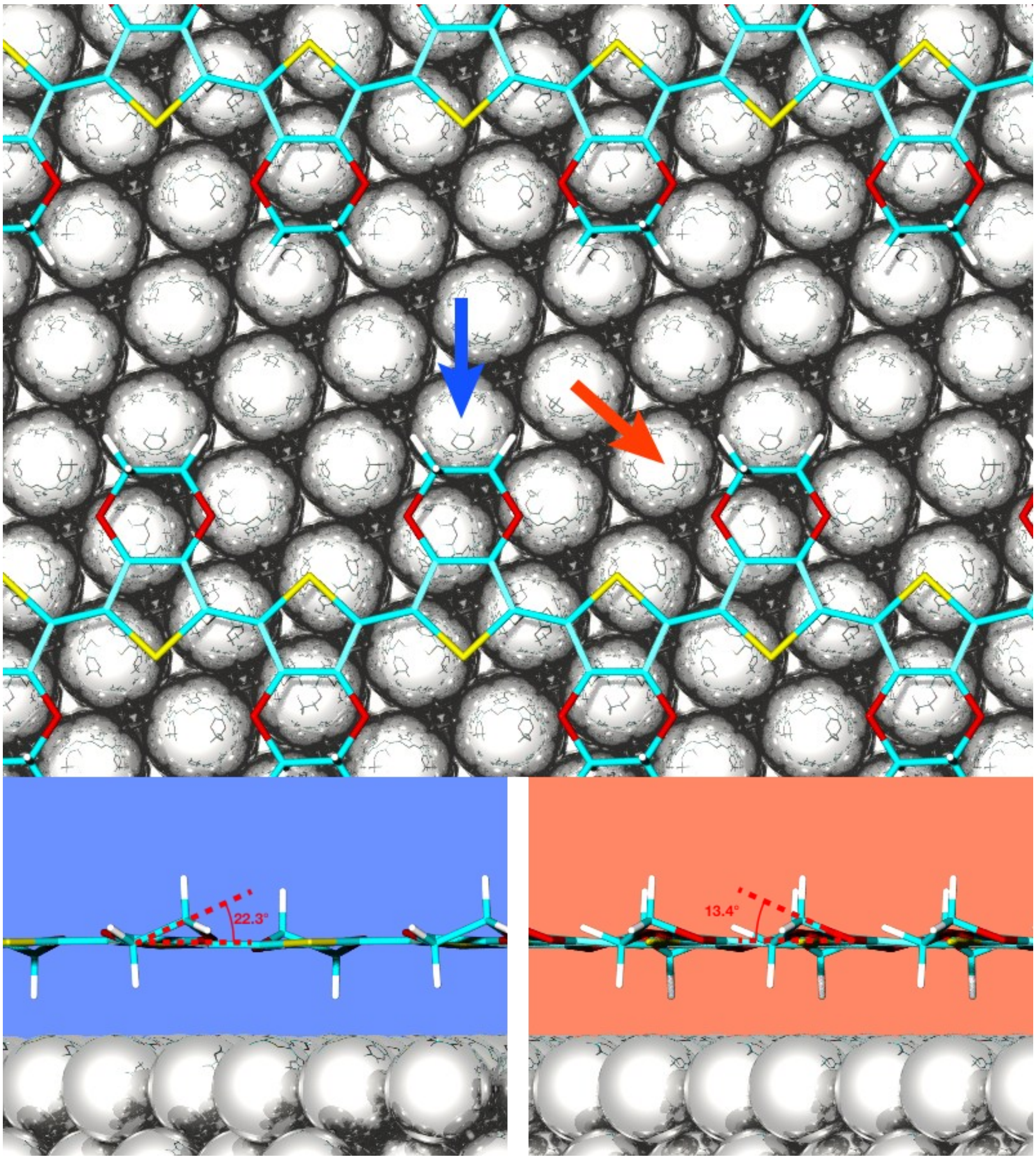

Figure 6: Computed geometry of PEDOT chains on Ag(111)

Calculated geometry for PEDOT on Ag(111)

The calculated geometry of the pEDOT system on Ag(111) is shown in Figure 6. The overlaid arrows in the top pane indicate the viewing angles along which each of the side views in the lower panels is projected. The geometry is found to be largely planar, save for the twisting of the ethylene group, as suggested by the NEXAFS spectra. The calculated geometry finds a tilt of 22.3° of the C-C bond in the ethylene group with respect to the plane of the surface, and a tilt of tilt of the γC-O bonds of 13.4° from the surface plane in order to enable the γ-carbon geometry. The coordinates for the energy-minimised periodic cell are given below in crystallographic information file (CIF) format.

```
#======================================================================

# CRYSTAL DATA

#----------------------------------------------------------------------

data_VESTA_phase_1


_pd_phase_name                         'XCrySDen XSF file'
_cell_length_a                         7.96358
_cell_length_b                         15.92717
_cell_length_c                         29.49139
_cell_angle_alpha                      90
_cell_angle_beta                       90
_cell_angle_gamma                      59.99999
_symmetry_space_group_name_H-M         'P 1'
_symmetry_Int_Tables_number            1

loop_
_symmetry_equiv_pos_as_xyz
   'x, y, z'

loop_
   _atom_site_label
   _atom_site_occupancy
   _atom_site_fract_x
   _atom_site_fract_y
   _atom_site_fract_z
   _atom_site_adp_type
   _atom_site_B_iso_or_equiv
   _atom_site_type_symbol
   Ag1      1.0   0.761836    0.095263    0.333352   Biso  1.000000 Ag
   Ag2      1.0   0.333352    0.166675    0.333352   Biso  1.000000 Ag
   Ag3      1.0   0.904814    0.238086    0.333352   Biso  1.000000 Ag
   Ag4      1.0   0.476204    0.309497    0.333352   Biso  1.000000 Ag
   Ag5      1.0   0.047595    0.380981    0.333352   Biso  1.000000 Ag
   Ag6      1.0   0.618985    0.452393    0.333352   Biso  1.000000 Ag
   Ag7      1.0   0.190447    0.523804    0.333352   Biso  1.000000 Ag
   Ag8      1.0   0.761910    0.595215    0.333352   Biso  1.000000 Ag
   Ag9      1.0   0.333353    0.666699    0.333352   Biso  1.000000 Ag
   Ag10     1.0   0.904812    0.738062    0.333352   Biso  1.000000 Ag
   Ag11     1.0   0.476130    0.809546    0.333352   Biso  1.000000 Ag
   Ag12     1.0   0.047593    0.880957    0.333352   Biso  1.000000 Ag
   Ag13     1.0   0.619109    0.952368    0.333352   Biso  1.000000 Ag
   Ag14     1.0   0.190446    0.023780    0.333352   Biso  1.000000 Ag
   Ag15     1.0   0.952407    0.119043    0.416664   Biso  1.000000 Ag
   Ag16     1.0   0.523797    0.190454    0.416664   Biso  1.000000 Ag
   Ag17     1.0   0.095187    0.261938    0.416664   Biso  1.000000 Ag
   Ag18     1.0   0.666578    0.333350    0.416664   Biso  1.000000 Ag
   Ag19     1.0   0.238040    0.404761    0.416664   Biso  1.000000 Ag
   Ag20     1.0   0.809503    0.476172    0.416664   Biso  1.000000 Ag
   Ag21     1.0   0.381019    0.547584    0.416664   Biso  1.000000 Ag
   Ag22     1.0   0.952283    0.619067    0.416664   Biso  1.000000 Ag
```

Ag23	1.0	0.523799	0.690479	0.416664	Biso	1.000000	Ag
Ag24	1.0	0.095186	0.761914	0.416664	Biso	1.000000	Ag
Ag25	1.0	0.666701	0.833325	0.416664	Biso	1.000000	Ag
Ag26	1.0	0.238164	0.904737	0.416664	Biso	1.000000	Ag
Ag27	1.0	0.809429	0.976220	0.416664	Biso	1.000000	Ag
Ag28	1.0	0.380944	0.047632	0.416664	Biso	1.000000	Ag
Ag29	1.0	0.996150	0.999528	0.498846	Biso	1.000000	Ag
Ag30	1.0	0.568140	0.070511	0.499023	Biso	1.000000	Ag
Ag31	1.0	0.138817	0.142197	0.498951	Biso	1.000000	Ag
Ag32	1.0	0.710145	0.213443	0.499162	Biso	1.000000	Ag
Ag33	1.0	0.281510	0.284643	0.498672	Biso	1.000000	Ag
Ag34	1.0	0.852639	0.356490	0.498507	Biso	1.000000	Ag
Ag35	1.0	0.423229	0.428393	0.499699	Biso	1.000000	Ag
Ag36	1.0	0.995564	0.500264	0.498241	Biso	1.000000	Ag
Ag37	1.0	0.566921	0.570847	0.499780	Biso	1.000000	Ag
Ag38	1.0	0.138293	0.642302	0.499973	Biso	1.000000	Ag
Ag39	1.0	0.709997	0.713381	0.499940	Biso	1.000000	Ag
Ag40	1.0	0.281988	0.784084	0.498402	Biso	1.000000	Ag
Ag41	1.0	0.853556	0.856000	0.499614	Biso	1.000000	Ag
Ag42	1.0	0.424820	0.927390	0.499038	Biso	1.000000	Ag
H1	1.0	0.998146	0.417561	0.583605	Biso	1.000000	H
H2	1.0	0.213736	0.864761	0.585363	Biso	1.000000	H
C1	1.0	0.995741	0.416116	0.620905	Biso	1.000000	C
H3	1.0	0.861217	0.478382	0.633099	Biso	1.000000	H
S1	1.0	0.783123	0.216587	0.628929	Biso	1.000000	S
O1	1.0	0.987588	0.330560	0.635413	Biso	1.000000	O
C2	1.0	0.162982	0.246185	0.631793	Biso	1.000000	C
C3	1.0	0.184334	0.154670	0.632566	Biso	1.000000	C
O2	1.0	0.351495	0.330494	0.625699	Biso	1.000000	O
C4	1.0	0.031503	0.128296	0.632821	Biso	1.000000	C
C5	1.0	0.343960	0.246154	0.628175	Biso	1.000000	C
S2	1.0	0.432860	0.066125	0.629467	Biso	1.000000	S
H4	1.0	0.181953	0.478097	0.627619	Biso	1.000000	H
C6	1.0	0.505232	0.154639	0.627025	Biso	1.000000	C
C7	1.0	0.710962	0.127915	0.627199	Biso	1.000000	C
C8	1.0	0.053027	0.036742	0.632729	Biso	1.000000	C
C9	1.0	0.219709	0.866695	0.622625	Biso	1.000000	C
C10	1.0	0.872199	0.036515	0.629318	Biso	1.000000	C
C11	1.0	0.172561	0.416062	0.640456	Biso	1.000000	C
O3	1.0	0.228695	0.952500	0.636267	Biso	1.000000	O
O4	1.0	0.864859	0.952019	0.628085	Biso	1.000000	O
H5	1.0	0.355345	0.804637	0.634454	Biso	1.000000	H
H6	1.0	0.034630	0.804563	0.631914	Biso	1.000000	H
C12	1.0	0.044225	0.867395	0.643398	Biso	1.000000	C
H7	1.0	0.168467	0.417634	0.677736	Biso	1.000000	H
H8	1.0	0.049656	0.868128	0.680662	Biso	1.000000	H

References

1. E. Gann, C. R. McNeill, A. Tadich, B. C. Cowie and L. Thomsen, *Journal of synchrotron radiation*, 2016, **23**.
2. I. Horcas, R. Fernández, J. Gomez-Rodriguez, J. Colchero, J. Gómez-Herrero and A. Baro, *Review of Scientific Instruments*, 2007, **78**, 013705.
3. P. Giannozzi, S. Baroni, N. Bonini, M. Calandra, R. Car, C. Cavazzoni, D. Ceresoli, G. L. Chiarotti, M. Cococcioni and I. Dabo, *Journal of physics: Condensed matter*, 2009, **21**, 395502.
4. J. P. Perdew, K. Burke and M. Ernzerhof, *Physical review letters*, 1996, **77**, 3865.

5. M. Dion, H. Rydberg, E. Schröder, D. C. Langreth and B. I. Lundqvist, *Physical review letters*, 2004, **92**, 246401;
T. Thonhauser, V. R. Cooper, S. Li, A. Puzder, P. Hyldgaard and D. C. Langreth, *Physical Review B*, 2007, **76**, 125112;
G. Román-Pérez and J. M. Soler, *Physical review letters*, 2009, **103**, 096102.
6. J. Tersoff and D. Hamann, in *Scanning Tunneling Microscopy*, Springer, 1985, pp. 59.

Please do not adjust margins